

# CONSTRAINING THE DARK CUSP IN THE GALACTIC CENTER BY LONG-PERIOD BINARIES

TAL ALEXANDER

Dept. of Particle Physics & Astrophysics, Weizmann Institute of Science, P.O. Box 26, Rehovot 76100, Israel

AND

OLIVER PFUHL

Max-Planck-Institut für extraterrestrische Physik, Postfach 1312, Garching D-85741, Germany.

*Draft version May 20, 2018*

## Abstract

Massive black holes (MBHs) in galactic nuclei are believed to be surrounded by a high density stellar cluster, whose mass is mostly in hard-to-detect faint stars and compact remnants. Such dark cusps dominate the dynamics near the MBH: a dark cusp in the Galactic center (GC) of the Milky Way would strongly affect orbital tests of General Relativity there; on cosmic scales, dark cusps set the rates of gravitational wave emission events from compact remnants that spiral into MBHs, and they modify the rates of tidal disruption events, to list only some implications. A recently discovered long-period massive young binary ( $P_{12} \lesssim 1$  yr,  $M_{12} \sim \mathcal{O}(100 M_{\odot})$ ,  $T_{12} \sim 6 \times 10^6$  yr), only  $\sim 0.1$  pc from the Galactic MBH (Pfuhl et al. 2013), sets a lower bound on the 2-body relaxation timescale there,  $\min t_{\text{rlx}} \propto (P_{12}/M_{12})^{2/3} T_{12} \sim 10^7$  yr, and correspondingly, an upper bound on the stellar number density,  $\max n_{\star} \sim \text{few} \times 10^8 / \langle M_{\star}^2 \rangle \text{ pc}^{-3}$ , based on the binary's survival against evaporation by the dark cusp. However, a conservative dynamical estimate, the drain limit, implies  $t_{\text{rlx}} > \mathcal{O}(10^8 \text{ yr})$ . Such massive binaries are thus too short-lived and tightly bound to constrain a dense relaxed dark cusp. We explore here in detail the use of longer-period, less massive and longer-lived binaries ( $P_{12} \sim \text{few yr}$ ,  $M_{12} \sim 2 - 4 M_{\odot}$ ,  $T_{12} \sim 10^8 - 10^{10}$  yr), presently just below the detection threshold, for probing the dark cusp, and develop the framework for translating their future detections among the giants in the GC into dynamical constraints.

*Subject headings:* black hole physics — Galaxy: center — stellar dynamics — infrared: stars — binaries: general

## 1. INTRODUCTION

The dynamical state of the stellar cluster around the massive black hole (MBH) in the Galactic Center (GC), and the mechanisms that determine it, are of interest because such systems are ubiquitous in the universe, and because the GC is by far the most observationally accessible of them. The key question is whether the GC is dynamically relaxed (Alexander 2011a). An unrelaxed system reflects its particular formation history. In contrast, the properties of a relaxed system can be understood and modeled from first principles, independently of initial conditions, and extrapolated to other relaxed galaxies. The GC, like other galactic nuclei with low-mass MBHs, is expected to be dynamically relaxed if it evolved passively in isolation (Bar-Or et al. 2013), and consequently to have a centrally concentrated power-law stellar cusp, with a density profile  $\propto r^{\alpha}$ , where  $\alpha \sim 3/2 - 5/2$  (Bahcall & Wolf 1977; Alexander & Hopman 2009; Keshet et al. 2009) (Figure 1). However, recent photometric and spectroscopic studies of the stellar distribution in the GC (Buchholz et al. 2009; Do et al. 2009; Bartko et al. 2010) indicate that the radial density profile of the spectroscopically identified low-mass red giants on the  $\sim 0.5$  pc scale, thought to trace the long-lived population there, rises inward much less steeply than expected in steady state, or even decreases toward the center.

The core in the spatial distribution of the old red giants could still be consistent with a relaxed GC, if some mechanism selectively destroys giants, or rejuvenates them to appear as hot stars (see review by Alexander 2005). However, all such processes proposed to date (e.g. envelope stripping by star-giant collisions, Alexander 1999; Bailey & Davies 1999; tidal heating, Alexander & Morris 2003) are ineffec-

tive outside the central  $\sim 0.1$  pc. The simplest interpretation for the missing old cusp is that, contrary to expectations, the GC is not dynamically relaxed by two-body interactions. One possibility is that the cusp is continuously and rapidly drained into the MBH by faster competing dynamical processes (Madigan et al. 2011), in particular resonant relaxation (Rauch & Tremaine 1996). However, a recent exact derivation of the 2-body relaxation rate (Alexander 2011b; Bar-Or et al. 2013) suggest that it is fast enough to maintain a high density steady state cusp on the relevant spatial scales, even in the presence of resonant relaxation. Another possibility, which may well explain the observed cores in the light distributions of galaxies with more massive MBHs (Milosavljević et al. 2002), is that a cosmologically recent major merger event with another MBH carved out a central cavity in the stellar distribution (Merritt 2010). This would then mean that the GC has not evolved in isolation, and is not in steady state but still slowly evolving back to it.

There are however strong reasons to suspect that the GC is evolving at a rate faster than that of slow 2-body relaxation. The latest star formation episode in the GC formed  $\mathcal{O}(100)$  very massive stars (Paumard et al. 2006), which will likely leave behind stellar mass black holes (BHs). There are indications that a similar star formation episode occurred  $\mathcal{O}(10^8 \text{ yr})$  ago (Krabbe et al. 1995), as well as further indications of continuous star formation in the GC over a substantial fraction of the Hubble time on various spatial scales (Alexander & Sternberg 1999; Figer et al. 2004; Löffmann et al. 2010; Blum et al. 2003; Pfuhl et al. 2011). The estimated number of BHs produced in the inner parsec in the course of such a star formation history,  $\mathcal{O}(10^4)$ , is in itself large enough to lower the local relaxation time below

the Hubble time (Alexander 2011a). In addition, the massive gas structures presently observed just outside the MBH’s radius of influence at  $\sim 2$  pc (gas clumps and giant molecular clouds), act as massive perturbers (Perets et al. 2007) and can likewise lower the relaxation time below the Hubble time even well inside the radius of influence (Alexander 2011a). Even if the GC has undergone a cusp-scouring merger event, the re-formation rate of the mass-segregated cusp of stellar BHs is expected to be faster than that of the luminous, lower mass stars (Merritt 2010). In fact, numerical experiments indicate that the presence of a mass spectrum (not included in the analysis of Merritt 2010) accelerates the dynamics to the extent that the cusp can reform in substantially less than a Hubble time (Preto & Amaro-Seoane 2010), for a wide range of initial conditions.

The existence or absence of a dark cusp has important implications for processes that involve strong interactions with the MBH, such as the emission of gravitational waves from compact objects that inspiral into it (see review by Amaro-Seoane et al. 2007), the disruption of stars by the tidal field of the MBH and the resulting tidal flares (see review by Alexander 2012), and for the modeling of dynamics very close to MBHs (e.g. Hopman & Alexander 2006). A dark cusp around the Galactic MBH has crucial implications for the detection of relativistic effects in orbits of stars close to the Galactic MBH (the so called “S-cluster”) (Zucker et al. 2006; Merritt et al. 2010), in particular by future high precision interferometric experiments such as GRAVITY (Eisenhauer et al. 2008).

The discrepancy between the simplest interpretation of the observations and the theoretical expectations, and the absence of other lines of evidence for a major merger in the Milky Way’s past, suggests that the possibility that the observed red giants *do not* trace the total mass distribution, and that there *does exist* a dark cusp around the Galactic MBH, should be considered and tested empirically. The dynamical upper limits on the dark distributed mass within the S-cluster in the inner arcsec are still at least two orders of magnitude higher than expected from theoretical constraints (Gillessen et al. 2009a). Direct detection of the dark cusp in the GC, for example by gravitational lensing (Alexander & Loeb 2001; Chanamé et al. 2001) or by X-ray emission from accretion (Pessah & Melia 2003), is very difficult. The most promising approach to detect the faint stars and compact remnants appears to be through their dynamical interactions with other stars (e.g. Weinberg et al. 2005). There are hints that the resonant torques by such a cusp can explain some properties of the different sub-populations in the GC (Hopman & Alexander 2006), however the direct detection of these torques requires test stars on much shorter period orbits than are available at this time (e.g. Merritt et al. 2010).

We explore here a newly relevant dynamical method to probe the dark cusp in the GC: binary evaporation constraints. Relatively loosely-bound binaries are gradually detached by interactions with the field stars around them; for an assumed cusp model this then imposes limits on the properties of the surviving binary population (e.g. Perets 2009a; Hopman 2009). Here we invert the constraints, and use the existence of binaries in the GC to place upper limits on the product of the total number density and the second moment of the mass distribution,  $n_\star \langle M_\star^2 \rangle$ , or equivalently, a lower limit on the relaxation time  $t_{\text{rx}}$ , and thus constrain dynamical models of the GC. The challenge is to formulate the constraints in a

way that provides robust estimates in spite of statistical nature of evaporation and the uncertainty in the binary’s formation mechanism and dynamical age. It should be emphasized that although binaries can be destroyed by processes other than evaporation, this will not affect our estimates, which draw conclusions only from those binaries that do survive. These provide an upper limit on the effectiveness of each of the competing destruction mechanisms separately, evaporation included, and thereby allow constraining the physical parameters on which these processes depend.

The rest of this paper is organized as follows. The binary evaporation timescale and its relation to the 2-body energy relaxation timescale around a MBH are summarized in Sec. 2. Theoretical upper bounds and several specific stellar density models for the GC are presented in Sec. 3 to serve as benchmarks for evaluating the usefulness of binary evaporation constraints. The weak limits from the currently known massive GC binaries are estimated in Sec. 4, and the potential of lower-mass, longer-lived binaries to rule out density models is explored and discussed in detail. Finally, the prospects and difficulties of the binary evaporation method, both observational and theoretical, are discussed and summarized in Sec. 5.

## 2. EVAPORATION AND RELAXATION TIMESCALES

### 2.1. The binary evaporation timescale

In an isotropic, Keplerian power-law cusp near an MBH, where the stellar space density falls as  $n_\star \propto r^{-\alpha}$ , the Jeans equation implies that the 1D velocity dispersion is (e.g. Alexander 1999)

$$\sigma_\star^2(r) = v_\bullet^2(r)/(1 + \alpha), \quad (1)$$

where  $v_\bullet^2 = GM_\bullet/r$ . In a single mass population  $\alpha = 7/4$  (Bahcall & Wolf 1976), and the same holds for the most massive component of a multi-mass population (Bahcall & Wolf 1977), if it is the dynamically dominant one<sup>1</sup> (Alexander & Hopman 2009; Keshet et al. 2009). Unless stated otherwise, we adopt this value below. This velocity dispersion is in good agreement (to within 10%) with the one derived empirically by Trippe et al. (2008) for the old stellar population on the  $r = 0.01 - 0.5$  pc scale. Note that well within the radius of influence of the MBH ( $\sim 2$  pc in the GC), where the MBH dominates the potential, the stars are *not* in equipartition, as the velocity dispersion depends on the stellar mass only through the mass-dependence of the logarithmic slope,  $\alpha(M_\star)$ , which reflects mass segregation, and in steady state can vary between  $\alpha \sim 3/2 - 5/2$ . This limits the relative variations of  $\sigma_\star^2(M_\star)$  to less than  $\pm 15\%$  in  $\sigma_\star^2$  across the entire stellar mass range (typically 3 orders of magnitudes in mass) (Alexander & Kumar 2001). We therefore assume here that all stars, as well as the centers of mass (COM) of binaries, have the velocity dispersion given by Eq. (1).

A binary of mass  $M_{12} = M_1 + M_2$ , mass ratio  $q_m = M_2/M_1 \sim O(1)$  and binary semi-major axis (sma)  $a_{12} = -GM_1M_2/2E_{12}$  is considered “soft” when its binding energy  $|E_{12}|$  is less than the typical kinetic energy of the back-

<sup>1</sup> Many stellar populations can be approximated by a 2-mass mixture of heavy and light masses (stellar BHs with mass  $M_H \sim 10 M_\odot$  and number density  $n_H$  far from the MBH, versus all the rest with mass  $M_L \sim 1 M_\odot$ , and number density  $n_L$ ). In that case the relaxational parameter  $\Delta = 4/(3 + M_H/M_L)(n_H M_H^2)/(n_L M_L^2)$  determined whether the relaxed steady state is in the strong segregation limit ( $\Delta \ll 1$  and  $\alpha_H = 11/4$ ) or the weak segregation limit ( $\Delta \gg 1$  and  $\alpha_H = 7/4$ ) (Alexander & Hopman 2009).

ground stars of mean mass  $\langle M_\star \rangle$  (e.g. Heggie 1975),

$$s \equiv \frac{|E_{12}|}{\langle M_\star \rangle \sigma_\star^2} = \frac{1 + \alpha}{2} \frac{M_1 M_2}{M_\bullet \langle M_\star \rangle} \frac{r}{a_{12}} \simeq \frac{1}{8} \frac{M_{12}}{\langle M_\star \rangle} \frac{v_{12}^2}{\sigma_\star^2} < 1, \quad (2)$$

where  $r$  is taken to be the typical radius of the binary's orbit around the MBH,  $v_{12}^2 \equiv GM_{12}/a_{12}$ , and the last approximate equality assumes  $q_m = 1$ . The parameter  $s$  is the softness parameter—the smaller  $s$  is, the softer (relatively less bound) the binary. Statistically, interactions with field stars make soft binaries softer, until they become unbound, while hard binaries become harder, until they merge (Heggie 1975). The present-day value of the softness parameter,  $s_0$ , can be estimated for an assumed stellar density model ( $\alpha$  and  $\langle M_\star \rangle$ ) from the observationally deduced properties of the binary ( $M_{12}$ ,  $a_{12}$  and  $r$ ).

The evaporation timescale for soft binaries, whose COM velocity dispersion is parametrized as  $\sigma_{12}^2 = \sigma_\star^2/q_\sigma$  (in equipartition,  $q_\sigma = M_{12}/M_\star$ , but near a MBH,  $q_\sigma \simeq 1$ ), is generally<sup>2</sup>

$$\begin{aligned} \tau_{\text{evap}} &\equiv \frac{|E_{12}|}{\langle D(\Delta E) \rangle} = \frac{1}{8} \sqrt{\frac{1 + q_\sigma}{2\pi q_\sigma}} \frac{M_{12} \sigma_\star(r)}{G n_\star \langle M_\star^2 \rangle a_{12} \log \Lambda_{12}(r)} \\ &\simeq 0.07 \frac{v_{12}^2 \sigma_\star(r)}{G^2 n_\star \langle M_\star^2 \rangle \log \Lambda_{12}(r)} \quad (\text{for } q_\sigma = 1), \quad (3) \end{aligned}$$

where  $E_{12}$  is the *present-time* orbital energy,  $\langle D(\Delta E) \rangle$  is the mean (i.e. averaged over binary COM velocities) energy diffusion coefficient due to interactions of the binary with field stars,  $n_\star$  is the total stellar number density, and  $\langle M_\star^2 \rangle = n_\star^{-1} \int dM_\star (dn_\star/dM_\star) M_\star^2$  is the second moment of the mass-function.  $\langle M_\star^2 \rangle$  is usually dominated by the heaviest mass in the mass spectrum (likely the stellar-mass BHs)<sup>3</sup>, so that  $n_\star \langle M_\star^2 \rangle \gtrsim n_{bh} M_{bh}^2$ . At fixed binary mass, the evaporation timescale scales approximately as  $\tau_{\text{evap}} \propto \langle M_\star^2 \rangle^{-1}$ .

The Coulomb factor for evaporation in the soft limit,  $\Lambda_{12} = b_{\text{max}}/b_{\text{min}}$ , is estimated by setting the maximal impact parameter to  $b_{\text{max}} = a_{12}/2$ , so that the interaction will be with only one of the binary members, and not with the binary's COM, and the minimal one at the strong deflection limit  $b_{\text{min}} = G(M_1 + M_\star)/\langle v_{\text{rel}}^2 \rangle$ , where the typical relative velocity for an encounter with a member star of a soft binary is  $\langle v_{\text{rel}}^2 \rangle = 3\sigma_\star^2 + 3\sigma_{12}^2 = 3(1 + 1/q_\sigma)\sigma_\star^2$ . Therefore,

$$\Lambda_{12} \sim 3 \left( \frac{1 + 1/q_\sigma}{1 + 2/q_\sigma} \right) \frac{\sigma_\star^2(r)}{v_{12}^2} = 2 \frac{\sigma_\star^2(r)}{v_{12}^2} \simeq \frac{1}{4} \frac{M_{12}}{\langle M_\star \rangle} \frac{1}{s(r)}, \quad (4)$$

where  $q_\sigma = 1$  is assumed, and the last approximate equality also assumes  $q_m = 1$ .

Note that since binary evaporation requires that the perturber's distance of closest approach be closer to one star than to the binary's center of mass, the contribution of extended massive perturbers, such as giant molecular clouds, to binary evaporation is substantially reduced (see discussion in Sec. 5).

The *timescale*  $\tau_{\text{evap}}$  is the present-time evaporation timescale evaluated using the observed sma. Since  $\langle D(\Delta E) \rangle$

<sup>2</sup> Generalizing the derivation of Binney & Tremaine (2008, Eq. 7.173), who assume  $M_{12} = 2M_\star$  and equipartition ( $q_\sigma = 2$ ). Note that Binney & Tremaine (1987) assumed  $q_\sigma = 1$ .

<sup>3</sup> For example, in the mass-segregated GC model of Alexander & Hopman (2009),  $n_\star \langle M_\star^2 \rangle = 1.24 n_{bh} M_{bh}^2 = 3.55 \times 10^7 M_\odot^2 \text{pc}^{-3}$  at  $r = 0.1 \text{pc}$ .

is independent of  $E_{12}$  (neglecting logarithmic terms), it follows that the *actual time* to evaporation,  $t_{\text{evap}}$ , is

$$t_{\text{evap}} \simeq \int_0^{E_{12}^0} \frac{dE}{\langle D(\Delta E) \rangle} \simeq \frac{E_{12}^0}{\langle D(\Delta E) \rangle_t} = \tau_{\text{evap}} \frac{E_{12}^0}{E_{12}}, \quad (5)$$

where  $E_{12}^0$  is the initial, unknown, binary energy and  $\langle D(\Delta E) \rangle_t$  is the time-weighted average of the diffusion coefficient over the binary's history<sup>4</sup>. Because the binary's evaporation is typically the result of many weak interactions, the scatter of the actual time to evaporation around the evaporation timescale is small,  $\Delta t_{\text{evap}}/\langle t_{\text{evap}} \rangle \ll 1$  (Perets et al. 2007).

Since soft binaries become softer, a maximal bound on  $t_{\text{evap}}$  can be obtained by assuming that the binary was initially as hard as it could be, with  $s = s_{\text{hard}}$ , which corresponded to the smaller of either the soft/hard boundary  $s = 1$ , or the hardest softness parameter possible, that of a contact binary with an initial sma  $a_{12}^0 = R_{\text{MS},1} + R_{\text{MS},2}$ , where  $R_{\text{MS}}$  is the radius of the star when still on the main sequence. We therefore set

$$s_{\text{hard}} = \min[1, s(r; a_{12} = R_{\text{MS},1} + R_{\text{MS},2})]. \quad (6)$$

Since  $s(t) \propto E_{12}(t)$  (Eq. 2), it follows that

$$t_{\text{evap}} \leq \tau_{\text{evap}} (s_{\text{hard}}/s_0) \equiv \tau_{\text{evap}} S_h, \quad (7)$$

where the maximal evolution ratio  $S_h > 1$  is the ratio of the maximal initial and present-day softness parameters. For low-mass binaries, where  $M_{12} \sim O(2 M_\odot)$  and  $R_{\text{MS}} \sim O(1 R_\odot)$ ,  $s_{\text{hard}} \sim 0.5 (\langle M_\star \rangle / 1 M_\odot)^{-1} (r/0.1 \text{pc})$ . We adopt below

$$t_{\text{evap}} = \tau_{\text{evap}} S_h, \quad (8)$$

as a conservative over-estimate of the evaporation time, which leads to a conservative under-estimate of the lower bound on the relaxation time (see Eq. 11).

## 2.2. The 2-body relaxation timescale

The local Chandrasekhar 2-body energy relaxation time (e.g. Spitzer 1987) is

$$\begin{aligned} t_{\text{rlx}} &= 0.34 \frac{\sigma_\star^3(r)}{G^2 n_\star \langle M_\star^2 \rangle \log \Lambda} \\ &\simeq \frac{0.68}{(3 - \alpha)(1 + \alpha)^{3/2}} \frac{M_\bullet^2}{\langle M_\star^2 \rangle} \frac{P(r)}{N_\star(r) \log \Lambda}, \quad (9) \end{aligned}$$

where  $N_\star(r)$  is the number of stars enclosed within  $r$ , and  $\Lambda \sim M_\bullet/M_\star$  (Bar-Or et al. 2013). Note that  $\Lambda \gg \Lambda_{12}$ , since in contrast to evaporation, encounters on all scales contribute to relaxation. It therefore follows that

$$t_{\text{rlx}} \simeq 4.8 \frac{\log \Lambda_{12}(r)}{\log \Lambda} \frac{\sigma_\star^2(r)}{v_{12}^2} \tau_{\text{evap}} \gg \tau_{\text{evap}}. \quad (10)$$

Thus a lower limit on the evaporation timescale translates to a lower limit on the 2-body relaxation time, and an upper limit on  $n_\star \langle M_\star^2 \rangle$ . An observed binary of period  $P_{12}$ , mass  $M_{12}$  and age  $T_{12} \leq t_{\text{evap}} \leq \tau_{\text{evap}} S_h$  at distance  $r$  from the MBH

<sup>4</sup> The binary's birth environment was likely much denser than its present day environment. However a red giant binary spends a negligible fraction of its lifetime there, and the uncertainty in the effective initial softness (the one it has after leaving its birth environment) is absorbed in the uncertainty in  $E_{12}^0$  (Eq. 8), and leads to a weaker lower bound on  $t_{\text{rlx}}$ .

implies therefore that the 2-body relaxation timescale there exceeds

$$\min t_{\text{rlx}}(r) \simeq 1.4 \frac{\log \Lambda_{12}(r) \sigma_*^2(r) T_{12}}{\log \Lambda v_{12}^2 S_h(r)}. \quad (11)$$

Note that the estimator  $\min t_{\text{rlx}}$  does not depend on  $\langle M_*^2 \rangle$ , as  $t_{\text{rlx}}$  does, but rather on the less sensitive  $\langle M_* \rangle$ , which enters weakly through the Coulomb logarithm<sup>5</sup>  $\log \Lambda = M_\bullet / \langle M_* \rangle$ , and more strongly through the factor  $S_h$ . All the other quantities that appear in  $\min t_{\text{rlx}}$  are directly observable or derivable:  $\log \Lambda_{12}$  (Eq. 4),  $\sigma_*$  (Eq. 1) and  $T_{12}$ . This lower bound can be used to rule out a specific density model for the GC, which predicts  $\alpha$  and  $\langle M_* \rangle$ . Alternatively, the uncertainty in  $\min t_{\text{rlx}}$  can be estimated by noting that when  $s_{\text{hard}} < 1$ ,  $\min t_{\text{rlx}} \propto R_{\text{MS}}(M_*) / \log(M_\bullet / M_*)$ , where  $R_{\text{MS}}(M_*) \propto M_*^\beta$ , with  $\beta = 1.25$  below  $\sim 1.5 M_\odot$ , at the transition between p-p to CNO cycle hydrogen burning, to  $\beta = 0.56$  above it (Schaller et al. 1992). The maximal range of  $\langle M_* \rangle$ , which lies between  $\sim 1 M_\odot$  (MS dwarfs) and  $\sim 10 M_\odot$  (stellar BHs), then implies the range in  $R_{\text{MS}}$  of  $\sim 1 R_\odot$  to  $R_{\text{MS}} \lesssim 10 R_\odot$  (for an  $O(100 M_\odot)$  BH progenitor), which translates to one order of magnitude uncertainty in  $\min t_{\text{rlx}}$ . When  $s_{\text{hard}} = 1$ ,  $\min t_{\text{rlx}} \propto 1 / \langle M_* \rangle \log(M_\bullet / M_*)$ .

The lower bound on the relaxation time translates into an upper bound on  $n_* \langle M_*^2 \rangle$  (Eqs. 9, 11),

$$\max(n_* \langle M_*^2 \rangle) \simeq 0.24 S_h(r) \frac{\sigma_*(r) v_{12}^2}{G^2 \log \Lambda_{12}(r) T_{12}}. \quad (12)$$

The estimate  $\max(n_* \langle M_*^2 \rangle)$  does not itself depend on  $\langle M_*^2 \rangle$ . An upper bound on the total stellar number density  $n_*$  can be obtained for an assumed value of  $\langle M_*^2 \rangle$ .

### 2.3. Binary formation by 3-body captures

The use of long-period binaries to constrain the dark cusp density requires reliable estimates of their *dynamical* age. For a primordial binary, the dynamical age equals the stellar age, which can be estimated from the binary’s luminosity and spectrum. However, when the binary is formed dynamically long after the stars are born, the dynamical age can only be bound from above by the stellar age. Such binaries can not provide strong constraints on the cusp density. Unless non-primordial binaries can be identified, their existence may be misinterpreted and lead to erroneous conclusions. However, as we argue here, such locally-formed binaries are expected to be extremely rare near a MBH. Another source of contamination, one that can not be decisively ruled out, is tidal capture of hierarchical triples in 4-body interactions with the MBH. This is discussed separately in Sec. 5.

Of the mechanisms generally considered for binary formation (e.g. Tohline 2002), those decoupled from the formation of the stars themselves are tidal capture in 2-body interactions and dynamical capture by 3-body interactions. Tidal capture is generally an inefficient process, leading to mergers rather than binary formation (see e.g. review by Benacquista 2006); it is very inefficient in galactic nuclei, since stellar encounters in the deep potential of a MBH are strongly hyperbolic—close encounters lead to mass-loss and spin-up, rather than

<sup>5</sup> The exact dependence of the Coulomb logarithm on the mass function has not yet been studied in detail, to the best of our knowledge.

capture (Alexander & Kumar 2001). Binary formation by 3-body capture requires that three stars to interact with mutual impact parameters of the order of  $b_{\pi/2} \sim GM_*/\sigma^2$  (Binney & Tremaine 2008, Eq. 7.10). This then allows strong interactions ( $\Delta v \sim v$ ) that extract a significant amount of relative kinetic energy from one pair and enable it to form a bound binary. The sma of the newly formed binary is expected to be also of order  $a_{12} \sim b_{\pi/2}$ . It then follows that a typical binary formed by 3-body capture is soft, with an initial softness parameters of  $s_0 \sim M_{12}/4 \langle M_* \rangle \sim 1/2 < 1$  (Eq. 2 with  $M_{12} = 2 \langle M_* \rangle$ ), as also suggested by the detailed analysis of 3-body capture in globular clusters (Goodman & Hut 1993). The formation rate is then  $\sim N_*(r)/t_3$ , where  $t_3$  is the typical timescale for a star to be involved in a 3-body capture interaction (Binney & Tremaine 2008, Eq. 7.11),

$$t_3 \sim \frac{\sigma_*^9}{n_*^2 G^5 M_*^5}. \quad (13)$$

The number of binaries formed by 3-body encounters on the spatial scale  $r$  over a time  $t$  a relaxation time (Eq. 9) is therefore

$$N_{12}(r; t) \sim N_*(r) \frac{t}{t_3} \sim N_*^2(r) \left( \frac{M_*}{M_\bullet} \right)^3 \frac{(1+\alpha)^3 t}{\log \Lambda t_{\text{rlx}}}. \quad (14)$$

After a Hubble time,  $t_H = 10$  Gyr,  $N_{12}(t_H) \sim 10^{-8} (t_H/t_{\text{rlx}}) \lesssim 10^{-6}$  for values typical of the GC ( $M_\bullet / \langle M_* \rangle \sim 10^6$  and  $N_*(r = 0.1 \text{ pc}) \sim 10^5$ ), and for the shortest realistic value for  $t_{\text{rlx}}$ ,  $\min t_{\text{rlx}}(0.1 \text{ pc}) > 10^8 \text{ yr}$  (see Sec. 3.1). The contribution of this formation channel to the binary population in the GC is therefore negligible (see also Hopman 2009).

## 3. STELLAR DENSITY MODELS FOR THE GALACTIC CENTER

To evaluate the practical relevance of GC binaries for constraining the dark cusp density, it is useful to have benchmarks for possible density profiles. We consider here a general dynamical upper bound on the cusp density, and two classes of specific models, one with a relaxed, high-density mass-segregated cusp, and the other with an unrelaxed low-density core.

### 3.1. Dynamical bounds on the dark cusp

Mass segregation models of the GC, which assume a passive evolution of the nuclear cluster, predict the accumulation of a steady state high density cusp of stellar remnants (Morris 1993). In steady state, the rate at which stars are scattered into the MBH from some volume  $< r$  is balanced by the rate at which stars are replenished by 2-body relaxation from outside  $r$ . The detailed calculation of the steady state density can be robustly bracketed by the conservative “drain limit” (Alexander & Livio 2004), which estimates the maximal number of objects that can survive against mutual 2-body scattering into the MBH over the age of the system. Taking the age of the system to be the Hubble time, the drain limit is the solution  $N_*(t = 0)$  of the condition

$$\frac{1}{N_*} \frac{dN_*}{dt} = \frac{1}{\log(\sqrt{2r/r_g}) t_{\text{rlx}}(r)} < \frac{1}{t_H}, \quad (15)$$

where  $r_g = GM_\bullet/c^2$  is the gravitational radius of the MBH. The drain limit corresponds to a minimal required survival

probability of 1/2 over a Hubble time, and it is only a function of  $\langle M_\star^2 \rangle$  (up to a logarithmic term<sup>6</sup>),

$$\max N_\star(< r) \sim \frac{2}{3} \frac{\log(\sqrt{2r/r_g})}{\log(M_\bullet/\langle M_\star \rangle)} \frac{M_\bullet^2}{\langle M_\star^2 \rangle} \frac{P(r)}{t_H}, \quad (16)$$

where  $P(r)$  is the orbital period around the MBH. It then follows that the shortest possible relaxation time in steady state, which is attained at the maximal density of the drain limit (substituting  $\max N_\star$  into Eq. 9), does not depend on the assumed mass function,

$$\min t_{\text{rlx, drain}} \simeq \frac{1}{(3-\alpha)(1+\alpha)^{3/2}} \frac{1}{\log(\sqrt{2r/r_g})} t_H, \quad (17)$$

For  $\alpha = 1.75$  this corresponds to

$$\min t_{\text{rlx, drain}} \simeq 2.5 \times 10^8 \text{ yr}. \quad (18)$$

Varying the assumed  $\alpha$  between  $\alpha = 0 \rightarrow 2$  changes the minimal relaxation time between  $2.4 \times 10^8$  yr (for  $\alpha = 7/5 = 1.4$ ) to a maximal one of  $4.7 \times 10^8$  yr (for  $\alpha = 0$ ).

The drain limit is a useful benchmark for our purpose since it provides an estimate of the shortest physically realizable relaxation time in steady state, which does not depend on detailed features of the Galactic model, such as the mass function and the boundary conditions. For example, the upper bounds on the enclosed number and density on the scale of the orbit of IRS 16NE, at  $r = 0.15$  pc (Sec. 4.1), are

$$\begin{aligned} \max N_\star &\sim 1.8 \times 10^4 \frac{(10 M_\odot)^2}{\langle M_\star^2 \rangle}, \\ \max n_\star &\sim 1.25 \times 10^6 \frac{(10 M_\odot)^2}{\langle M_\star^2 \rangle} \left( \frac{3-\alpha}{3} \right) \text{ pc}^{-3}. \end{aligned} \quad (19)$$

The drain limit is only a few times higher than the values derived by detailed calculations. For example, inside the inner  $\sim O(0.01)$  pc, the mass density of the GC is expected to be dominated by stellar mass BHs with mass  $M_{bh} \sim O(10 M_\odot)$  (Figure 2) (Freitag et al. 2006; Alexander & Hopman 2009), and in that case  $\langle M_\star^2 \rangle^{1/2} \sim M_{bh}$  and  $\max N_\star \sim \max N_{bh}$ . The drain limit on  $10 M_\odot$  stellar BHs in the inner 0.01 pc is  $\max N_{bh}(< 0.01 \text{ pc}) \simeq 250$ , compared to  $N_{bh}(< 0.01 \text{ pc}) \simeq 100$  derived by Fokker-Planck models, whether solved numerically (Alexander & Hopman 2009; see also Figure 1), or by the Hénon (Monte-Carlo) method (Freitag et al. 2006).

### 3.2. A relaxed mass-segregated high density cusp

The evolution of a galactic nucleus to a relaxed steady state configuration can be approximated in terms of the evolution of the stellar distribution function (DF) due to diffusion in phase space, and integrated in time from an arbitrary initial configuration to steady state by the Fokker-Planck (FP) equation. This scheme was first applied to a multi-mass system with a central MBH by Bahcall & Wolf (1977), with the approximations that the potential is Keplerian, the angular momentum diffusion is averaged, so that only diffusion in energy is integrated in time, and only non-coherent 2-body relaxation is considered. Two boundary conditions are imposed, one at

<sup>6</sup> Approximating  $t_{\text{rlx}} \sim \sigma^3/G^2 M_\star^2 n_\star \log \Lambda$ ,  $\sigma^2 \sim GM_\bullet/r$  and  $N_\star \sim (4\pi/3)n_\star r^3$ .

very high energy (close to the MBH), where the DF falls to zero, and one at the energy corresponding to the MBH's radius of influence ( $r_h \sim 2$  pc in the GC), where the stellar number density of each mass is fixed to some value, which reflects its population ratio far from the dynamical influences of the MBH, and therefore depends only on the assumed initial mass function (IMF) and the star-formation history.

Figure (1) shows results from such simple FP models for the GC, which assume present-day mass functions (PMFs) of stars and compact remnants that are derived by stellar population synthesis (Sternberg 1998) for continuous star-formation scenario for the GC (Alexander & Sternberg 1999; Figer et al. 2004), assuming two different IMFs (table 1). The first is based on the ‘‘universal’’ IMF (here approximated by the Miller & Scalo 1979 IMF, extending between  $M_\star = 0.1 M_\odot$  to  $120 M_\odot$ ), which reproduces the volume-averaged  $K$ -band luminosity of the luminous red giants in the inner few pc of the GC (Alexander & Sternberg 1999) and a second, extremely top-heavy model that is suggested by the population of the massive disk stars (Bartko et al. 2010), with  $dn_\star/dM_\star \propto M_\star^{-0.45}$  between  $M_\star = 0.8 M_\odot$  to  $120 M_\odot$ . The two IMFs result in very different stellar populations. While the mass and number of the universal IMF model are dominated by main sequence stars, and the BHs are only  $\sim 0.01$  of the mass and  $5 \times 10^{-4}$  of the number, the top-heavy IMF model is completely dominated by the compact remnants, with the BHs 0.89 of the mass and 0.57 of the number. Nevertheless, the relaxed steady states of both models conform with the drain limit (Figure 1B), which demonstrates its robustness.

A comparison of the density profiles of the BHs outside of the inner  $\sim 0.01$  pc in the two IMF models (Figure 1A) reveals the difference between the weak and strong mass-segregation regimes (Alexander & Hopman 2009). When the BHs, the most massive long-lived component in the mass function, are dominant in the population as they are in the top-heavy model<sup>7</sup>, they relax to an  $\alpha = 7/4$  cusp ( $n_\star \propto r^{-\alpha}$ ); when they are not, as in the universal model, they relax to a steeper slope, with  $\alpha \gtrsim 2$ . Closer to the MBH (here, at  $r \lesssim 0.01$  pc), mass segregation makes the BHs locally dominant, and both models converge to the  $\alpha = 7/4$  configuration.

Figure (2) shows the variation of the first and second mass moments ( $\langle M_\star \rangle$  and  $\langle M_\star^2 \rangle$ ) as function of distance from the MBH, for the two models, and provides convenient power-law approximations for  $\langle M_\star \rangle$ , for use in the minimal relaxation time estimate, Eq. (11).

### 3.3. An unrelaxed low-density Galactic core

The depleted numbers of red giants in the GC could be the result of a past merger event with another MBH, which dynamically ejected stars from the center (Merritt 2010). The resulting drastic decrease in the stellar density at the center would then increase the 2-body relaxation time well above the Hubble time, thereby slowing down the re-formation of a relaxed cusp. For certain choices of the initial radius of the evacuated region and of the time before present when the merger occurred, the slowly evolving post-merger GC density profile can match that observed today. Figure (6) shows the resulting 2-body relaxation time Merritt (2010), which substantially exceeds the Hubble time in the inner  $\sim 0.2$  pc of

<sup>7</sup> The top-heavy model has  $\Delta \simeq 40 \gg 1$  (weak segregation limit), whereas the universal model has  $\Delta \simeq 0.4 < 1$  (strong segregation limit), counting all stars and remnants with mass  $< 2 M_\odot$  as light (see footnote 1).

TABLE 1  
GC STELLAR PMF MODELS (UNSEGREGATED)

Stellar type	Typical mass	Universal IMF		Top-heavy IMF		Comments
		Mass fraction	Number fraction	Mass fraction	Number fraction	
Main sequence	$0.43 M_{\odot}/7.22 M_{\odot}^1$	0.73	0.85	0.03	0.03	Mean mass incl. remnants $0.48 M_{\odot}/6.38 M_{\odot}^1$
White dwarfs	$0.6 - 1.1 M_{\odot}$	0.23	0.14	0.02	0.14	Progenitor mass $2.5 - 8 M_{\odot}$
Neutron stars	$1.4 M_{\odot}$	0.03	0.01	0.06	0.26	Progenitor mass $8 - 30 M_{\odot}$
Black holes	$10 M_{\odot}$	0.01	0.0005	0.89	0.57	Progenitor mass $> 30 M_{\odot}$

<sup>1</sup> Average mass for the universal IMF and the top-heavy IMF, respectively.

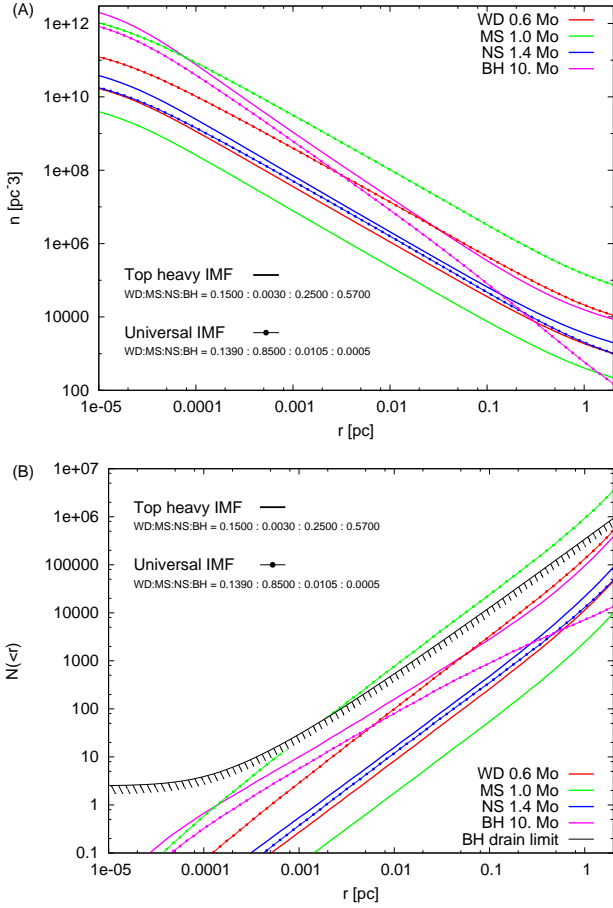


FIG. 1.— (A) Fokker-Planck steady-state mass-segregated density models for the GC (cf Alexander & Hopman 2009), assuming a simplified 4-component mass function ( $0.6 M_{\odot}$  white dwarfs,  $1 M_{\odot}$  main-sequence stars,  $1.4 M_{\odot}$  neutron stars and  $10 M_{\odot}$  stellar BHs). One model has the “universal” IMF (modeled here by the Miller & Scalo (1979) IMF), and the other has an extreme top-heavy IMF with  $dn_*/dM_* \propto M_*^{-0.45}$  between  $M_* = 0.8 M_{\odot}$  to  $120 M_{\odot}$ . The number ratios of the four components in each of the models are listed on the plot (see also table 1). (B) The cumulative number of stars in the universal and top-heavy GC models, are compared to each other and to the drain limit for stellar BHs, which both models obey.

the GC.

#### 4. BINARY EVAPORATION LIMITS ON THE DARK CUSP IN THE GC

##### 4.1. Long-period young massive binaries

The recently discovered long-period massive binary IRS 16NE (Pfuhl et al. 2013) at a projected distance of  $p = 3.05''$  (Paumard et al. 2006) has a period of  $P = 224.09 \pm 0.09$  days and a mass in the range  $80 M_{\odot} \lesssim M_{12} \lesssim 100 M_{\odot}$ , based

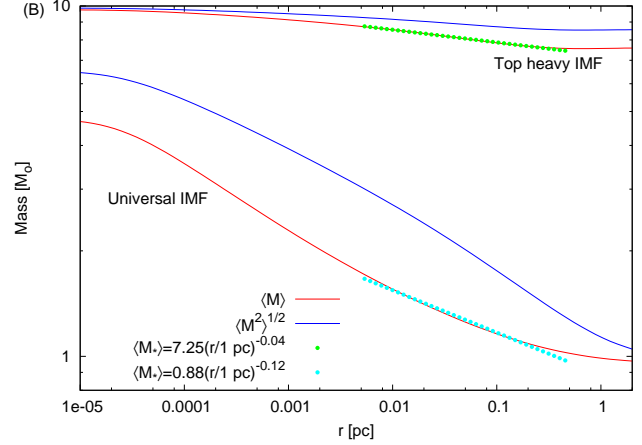


FIG. 2.— The first and second moments of the stellar mass,  $\langle M_* \rangle$  and  $\langle M_*^2 \rangle$ , as function of distance from the MBH in the two FP models for the GC (Figure 2). Also shown is a simple analytic approximation for  $\langle M_* \rangle$  in the range  $r = 0.005 - 0.5$  pc.

on the similarity of the observed spectrum of the primary to the known eclipsing binary IRS 16SW with  $M_1 \sim 50 M_{\odot}$  (Martins et al. 2006, 2007). The absence of spectral evidence for the secondary further suggests that  $M_2 \lesssim 30 M_{\odot}$ , so that the binary mass likely lies toward the lower limit of this mass range. IRS 16NE is a member of the clock-wise disk, a product of the recent star-burst episode, whose age is estimated at  $T = (6 \pm 2) \times 10^6$  yr (Paumard et al. 2006; Bartko et al. 2009; but see also younger age estimate by Lu et al. 2013).

We therefore adopt below a binary age of  $T_{12} = 6 \times 10^6$  yr and binary mass of  $M_{12} = 80 M_{\odot}$ , which translate to an sma  $a_{12} = 3.11$  AU and  $v_{12} = 151$  km s $^{-1}$  (for  $M_{12} = 100 M_{\odot}$ ,  $a_{12} = 3.26$  AU). The 3D distance of IRS 16NE and its eccentricity can be estimated using the inferred distance to the GC,  $R_0 \simeq 8.3$  kpc (Gillessen et al. 2009b), the binary’s observed plane-of-sky position and 3 components of the velocity, and by assuming that it is orbiting in the plane of the counter clockwise disk Paumard et al. (2006). It then follows that  $a \simeq 0.15$  pc $^8$  and  $e \simeq 0.14$  ( $r \simeq 0.13$  pc,  $v_{\bullet} \simeq 350$  km s $^{-1}$ ). Since the binary is on a nearly circular orbit, it is justified to substitute  $r = a$  and calculate the relevant timescales without orbital averaging. We further assume, based on the mass-segregated steady state model of the GC (Alexander & Hopman 2009), that the mean logarithmic slope at  $r = 0.15$  pc is  $\alpha = 1.5$ , and that  $\langle M_* \rangle = 1.2 M_{\odot}$  and  $\langle M_*^2 \rangle^{1/2} = 1.8 M_{\odot}$ . The Coulomb logarithm for evaporation is then  $\log \Lambda_{12} \simeq 1.46$ . According to the binary soft-

<sup>8</sup> A similar value is derived by assuming spherical symmetry, and estimating a 3D distance of  $r = \sqrt{3/2} p \approx 0.15$  pc.

ness criterion (Eq. 2), IRS 16NE is soft, or marginally soft, with  $s_0$  in the range 0.2 (for  $M_{12} = 80 M_\odot$  and  $\alpha = 0$ ) to 0.9 (for  $M_{12} = 100 M_\odot$  and  $\alpha = 2$ ). We therefore assume that the soft binary evaporation timescale is relevant for estimating the relaxation time scale. Since  $R_{\text{MS}}(50 M_\odot) = 9.5 R_\odot$  and  $R_{\text{MS}}(30 M_\odot) = 7.1 R_\odot$ ,  $s_{\text{hard}} = 1$ , and therefore the existence of IRS 16NE implies

$$\min t_{\text{rlx}}(\sim 0.15 \text{ pc}) \sim 2 \times 10^7 \text{ yr}. \quad (20)$$

The corresponding upper limit on the total number density

$$\max n_\star = \max(n_\star \langle M_\star^2 \rangle) / \langle M_\star^2 \rangle \sim 2 \times 10^8 \text{ pc}^{-3}. \quad (21)$$

Varying the assumed parameters over the range  $T_{12} = 4 \rightarrow 8 \text{ Myr}$ ,  $M_{12} = 50 \rightarrow 100 M_\odot$ ,  $\alpha = 0 \rightarrow 2$  changes  $\min t_{\text{rlx}}$  between  $\sim 1 \times 10^7 \text{ yr}$  (for  $\alpha = 2$ ,  $M_{12} = 50 M_\odot$  and  $T_{12} = 4 \times 10^6 \text{ yr}$ ) to  $\sim 6 \times 10^7 \text{ yr}$  (for  $\alpha = 0$ ,  $M_{12} = 100 M_\odot$  and  $T_{12} = 8 \times 10^6 \text{ yr}$ ). Such a short lower bound on the relaxation timescale lies well below the drain limit (Figure 5 B), and therefore cannot constrain realistic density models (see also Antonini et al. 2011). This conclusion is reinforced if instead  $\langle M_\star \rangle = 10 M_\odot$  is assumed, which further reduces  $\min t_{\text{rlx}}$  by a factor  $\mathcal{O}(10)$ .

#### 4.2. Long-period old low-mass binaries

Low-mass binaries have not yet been detected in the GC. Estimates of their numbers there are highly uncertain, given that star formation and dynamics in the unusual dense environment near a MBH are not well understood. The statistics of dense Galactic clusters could provide relevant estimates, as hinted by the finding of Pfuhl et al. (2013) that the number fraction of massive binaries in the GC ( $F_2 = 0.08\text{--}0.56$  at the 0.95 confidence level), which is consistent with that observed in dense Galactic OB clusters. Stellar clusters can provide relevant guidelines for low-mass binaries. Sollima et al. (2007) find in a sample of low-density Galactic globular clusters a low-mass binary fraction  $F_2 > 0.06$  in the cluster core, and globally  $F_2 \sim 0.1\text{--}0.5$  over the entire cluster. Sommariva et al. (2009) find a similar  $F_2 > 0.05$  lower limit on the binary fraction in the core, and  $F_2 > 0.03$  outside of it in globular cluster M4. Of these binaries, only a fraction can be actually detected. We now discuss the observational constraints, the red giant population in the GC, and the dynamical information that can be derived from the detection of long-period low mass binaries in the GC.

##### 4.2.1. Detection of long-period binaries in the GC

In order for a binary to be both detectable and useful for probing the density of the hypothetical dark cusp, it must satisfy several constraints.

(1) The binary's orbital period  $P_{12}$  should be short enough relative to the monitoring period, and the observing cadence high enough, so as to allow the extraction of the orbital parameters from the data,

$$\max P_{12} = \min 2\pi \sqrt{a_{12}^3 / GM_{12}} = x_P T_{\text{obs}}, \quad (22)$$

where the factor  $x_P$  depends on the detection mode. For spectroscopic binaries  $x_P \sim 1/2$ . However, for visual binaries a value as large as  $x_P \sim 10$  may be feasible, as discussed further below.

(2) The binary should be luminous enough to be observed with high S/N for reliable determination of the reflex velocity

(if observed as a spectroscopic binary) or proper motion (if observed as a visual binary), with a magnitude of

$$\max K < K_{S/N}, \quad (23)$$

where  $K$  is the magnitude of a single star.

(3) The binary's reflex motion or proper motion should be large enough to be measured with high S/N,

$$\min v_{12} = \min \sqrt{GM_{12}/a_{12}} > v_{S/N}. \quad (24)$$

(4) The binary should be dynamically sensitive to the relaxation timescales of interest, and at least to the conservative drain limit (Eq. 2). This would be the case if it is long-lived, with a main-sequence age  $T_{MS}$  such that (Eq. 11)

$$\min T_{MS} = \mathcal{O}(10) \frac{v_{12}^2}{v_\bullet^2(r)} S_h(r) t_{\text{rlx}} > \mathcal{O}(10) \frac{v_{12}^2}{v_\bullet^2(r)} t_{\text{rlx}}, \quad (25)$$

where  $S_h \geq 1$  is the ratio between the initial and present day softness parameter (Eq. 6).

(5) Long-lived low-mass main-sequence stars in the GC, with  $M_\star \lesssim 2 M_\odot$  are faint, with  $K_{MS} \gtrsim 19^9$ . This is still several magnitudes fainter than current limits for reliable spectroscopic identification<sup>10</sup>. Low-mass stars can only be observed in the giant phase, when their size expands to  $R_\star \sim \text{few} \times 10 R_\odot \sim \mathcal{O}(0.1 \text{ AU})$ . This limitation decreases the available targets by a factor of  $\sim 10$  (the typical ratio of the time spent in the giant phase relative to  $T_{MS}$ ), and imposes an additional requirement on the size of the orbit,  $R_\star < a_{12}/2$ , to avoid the hard-to-model complications of common envelope evolution, or equivalently,

$$\max v_{12} < v_\star, \quad (26)$$

where  $v_\star = \sqrt{GM_\star/R_\star}$  is the red giant's circular velocity, and  $M_\star \simeq M_{12}/2$  is assumed. For low-mass red giants,  $v_\star \sim \mathcal{O}(10^2 \text{ km s}^{-1})$ . However, these limitations are mitigated by the fact that red giants are advantageous for precise spectroscopic velocity determination since they are slow rotators and have sharp molecular absorption lines.

We now consider specifically the constraints imposed by present-day and upcoming observing capabilities of the VLT. It is straightforward to scale these constraints to other instruments and future capabilities.

Current observations of the GC with the SINFONI integral field spectrograph on the VLT (Eisenhauer et al. 2003; Bonnet et al. 2004) reach a radial velocity uncertainty of  $\lesssim 5 \text{ km s}^{-1}$  in a 1 hr integration for a  $K < K_{S/N} \simeq 14$  red giant. A  $3\sigma$  detection of the reflex motion then requires a radial velocity curve amplitude of  $V_r \gtrsim 15 \text{ km s}^{-1}$ . Assuming a circular orbit and the mean decrease by a factor  $\pi/4$  in the line-of-sight velocity due to the orbital inclination,  $v_{S/N} \simeq 20 \text{ km s}^{-1}$ . Since typically  $v_{S/N} < v_\star$ , the red giant size constraint (Eq. 26) is not a limitation. The minimal useful main-sequence lifetime can be estimated by

<sup>9</sup> For  $DM_{GC} = 14.6$  (Gillessen et al. 2009b) and  $A_K = 2.7$  (Fritz et al. 2011), taking  $M_K(2 M_\odot) = 1.6$  and  $M_K(1 M_\odot) = 3.75$  (adapted from Schaller et al. (1992) ZAMS models for  $Z = 0.02$ ).

<sup>10</sup> The photometric detection limit in the GC is  $K \sim 19$  (Schödel et al. 2007). Due to stellar crowding, the detection completeness starts to be affected already at a magnitude of  $K < 17$  (Schödel et al. 2007). The faintest stars that have been spectroscopically identified in the GC are  $K \sim 17.6$  (Pfuhl et al. 2011), yet with an integration time of  $\sim 10 \text{ hr}$  and low signal-to-noise. Typical integration times of 1-2 hr allow the spectroscopic identification of stars with  $K \sim 14\text{--}15$  (e.g. Bartko et al. 2010).

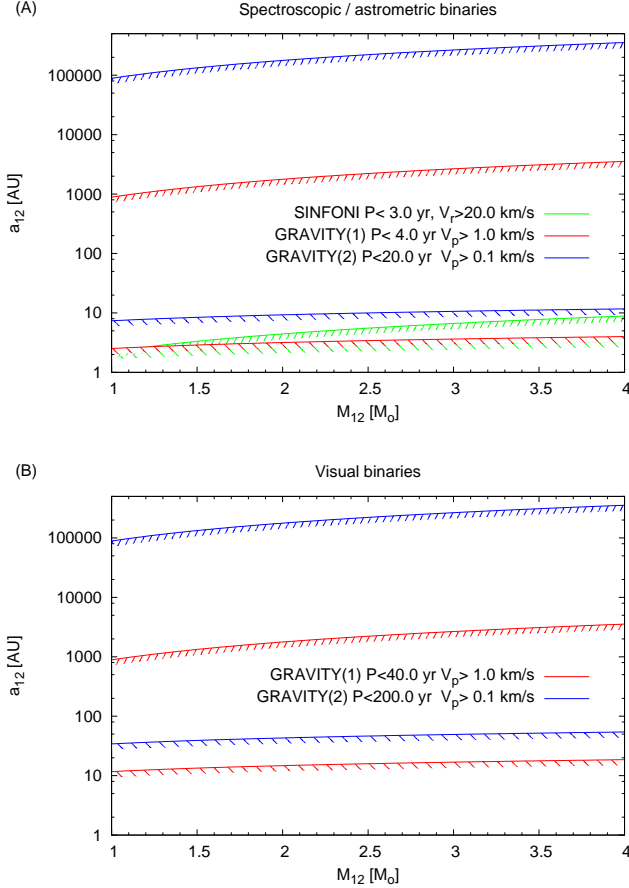


FIG. 3.— (A) The detectability limit on the binary mass  $M_{12}$  and sma  $a_{12}$  for spectroscopic / astrometric binaries, for the current period and velocity limits of SINFONI ( $P < 3$  yr and  $V_p > 20$  km s $^{-1}$  for  $e = 0$  and  $\sin i = 1$ ) and for future limits of GRAVITY (Case 1: conservative  $P < 4$  yr and  $V_p > 1$  km s $^{-1}$ . Case 2: optimistic  $P < 20$  yr and  $V_p > 0.1$  km s $^{-1}$ , for  $e = 0$ ), in the low-mass range where binaries are long-lived enough to probe relaxation (Eq. 25). Binaries are detectable in the region that is below the lower of the max  $P_{12}$  upper bound (coarse hashes) and the min  $V$  upper bound (fine hashes) for each of the three cases. (B) The same as above, for visual binaries observed by GRAVITY.

taking  $v_{12}$  in the range  $v_{S/N}$  to  $v_*$  (Eq. 25). For example, for  $r = 0.15$  pc, where  $\min t_{\text{rlx, drain}} \simeq 2.5 \times 10^8$  yr (Sec. 3.1),  $\min T_{MS} \sim 8 \times 10^6 - 2 \times 10^8$  yr, which corresponds to a maximal useful mass in the range  $\max M_* \sim 4 - 20 M_{\odot}$  Schaller et al. (1992). More realistic dynamical models with  $t_{\text{rlx}} > \min t_{\text{rlx, drain}}$  (Sec. 3) limit  $\max M_*$  to the lower boundary of this range.

Observations of the GC with SINFONI have been on-going for  $T_{\text{obs}} \sim 10$  years now, mostly focused on the central 0.2 pc, and spaced between several days to several years. This limits currently detectable binaries to periods of at most  $\max P_{12} = T_{\text{obs}}/2 \sim 5$  yr, and realistically probably to  $\lesssim 3$  yr. The joint constraints of  $\max P_{12}$  and  $\min V_r$  (Eqs. 22, 24) translate to joint constraints on the binary mass and sma,

$$\begin{aligned} a < a_P &= \sqrt[3]{GM_{12}(2\pi \max P_{12})^2}, \\ a < a_{V_r} &= GM_{12} \sin^2 i / \min V_r^2, \end{aligned} \quad (27)$$

where  $a_{V_r}$  is estimated conservatively for a circular orbit.

The upcoming AO-assisted IR interferometer GRAVITY

(Eisenhauer et al. 2011) will allow the detection of binaries with separations up to several AU. The instrument will provides two detection regimes: Detection by fully resolving the two stars (“visual binaries”), and detection by the shift of the binary’s photo-center (“astrometric binaries”). GRAVITY’s astrometry will reach a precision of  $10 \mu\text{as}$  (0.08 AU). Over a 4 year period this will allow the measurement of proper velocities and accelerations at precisions of  $\mu \sim 10 \mu\text{as yr}^{-1}$  ( $V_p \sim 0.4$  km s $^{-1}$ ) and  $\dot{\mu} \sim 10 \mu\text{as yr}^{-2}$  ( $dV_p/dt \sim 1.25 \times 10^{-8}$  km s $^{-2}$ ), respectively, on sources as faint as  $K_{S/N} \sim 16$  (Bartko et al. 2008; Eisenhauer et al. 2011). Over 10 years these will improve to  $\mu \sim 2 \mu\text{as yr}^{-1}$  ( $V_p \sim 0.08$  km s $^{-1}$ ) and  $\dot{\mu} \sim 2 \mu\text{as yr}^{-2}$  ( $dV_p/dt \sim 2.5 \times 10^{-9}$  km s $^{-2}$ ). We conservatively assume below  $T_{\text{obs}} = 4$  yr, but also consider the optimistic case of  $T_{\text{obs}} = 20$  yr.

*Visual binaries*— The high resolution of the VLTI allows to resolve binaries with separations  $> 1$  mas (8 AU at the distance of the GC). We will refer to these binaries as visual binaries, since their separation can be directly measured as in classical imaging. The typical orbital time for a  $M_{12} = 2 M_{\odot}$  binary with a separation of 8 AU is 16 yr; for a separation of 25 AU it is 83 yr. This realistically implies coverage of only a fraction of the orbit. However, this in itself will not prevent the detection of such long-period binaries. Even in the dense environment of the central cluster, the probability of a chance alignment of two stars at a projected distance of 1 mas (8 AU) from each other is  $\mathcal{O}(10^{-6})$  and for 3 mas (25 AU) it is  $\mathcal{O}(10^{-5})$  (Eq. 29). Consequently, pairs detected at separations of  $\lesssim$  few  $\times 10$  AU are true binaries at a very high confidence, and their detection can already constrain the relaxation time even without orbital information. Measurements of acceleration over arcs of the orbit can then be used to derive the orbital parameters. Guided by such analysis of partial orbits by Cvetković & Novaković (2010), we will assume here that orbits as long as  $\max P_{12} = 10T_{\text{obs}}$  can be solved. The minimal detectable plane-of-sky velocity amplitude  $\min V_p$  then translates to the additional constraint of

$$a < a_{V_p} = GM_{12} / \min V_p^2, \quad (28)$$

where again  $a_{V_p}$  is estimated conservatively for a circular orbit.

Note that such long-period orbits somewhat relax the constraint on the maximal mass useful for probing the dynamics<sup>11</sup>, since on such softer orbits even shorter-lived stars can still provide interesting dynamical constraints on the dark cusp.

*Astrometric binaries*— GRAVITY’s novel astrometric mode will make it possible to detect unresolved binaries by the astrometric shift of their common photo-center, provided they have unequal fluxes. This requirement will most likely be satisfied even for the fiducial near-equal mass red giant binaries that are assumed in our analysis. Even a small difference in the mass leads to a large difference in luminosity, and even more so, a small difference in the post-main sequence evolutionary stage, as can be demonstrated, for example, by the median visual magnitude difference of  $\Delta m \simeq 0.65$ , observed in binaries of (Hartkopf & Mason 2001). Although the amplitude of the photo-center shift is  $\sim \Delta m$  times smaller than the true orbital motion of the brighter component, it

<sup>11</sup>  $\max M_* \propto a_{12}^{2/7}$  since  $\min T_{MS} \propto M_{12}/a_{12}$  (Eq. 25) and  $T_{MS}(M_*) \propto M_*^{-5/2}$  for  $M_* \lesssim 10 M_{\odot}$ .

does contain additional constraints on the orbit beyond those provided by spectroscopy alone. The detailed methodology for dealing with astrometric binaries will be discussed elsewhere. Here we simplify the analysis by ignoring the photocenter shift, and treat the binary detectability limits for the GRAVITY astrometric mode in a similar way as those of spectroscopic binaries. Following the criteria suggested by Hartkopf & Mason (2001), we restrict ourselves to binaries with  $\max P_{12} = T_{\text{obs}}$ .

Figure (3) shows the range of binary mass and sma where spectroscopic binaries are now detectable with SINFONI, and where astrometric and visual binaries will be detectable in the future with GRAVITY (for both the conservative and optimistic sets of assumptions), focusing on the low-mass range that is relevant for testing the dynamical state of the GC. The limiting factor in all cases is the maximal binary period required for detection and orbital parameter derivation. For spectroscopic SINFONI binaries and for astrometric GRAVITY binaries in the conservative case, the binary sma is limited to  $\max a_{12} \sim 3$  AU. We therefore conclude that in this case the big improvement in astrometric sensitivity by GRAVITY will not increase discovery space by much, but will rather allow much better determination of the orbital parameters. GRAVITY's advantage will be most significant in the optimistic case, where the monitoring extends over much longer periods, or for visual binaries. In that case discovery space will increase to  $\max a_{12} \sim 10$  AU for both astrometric binaries and visual binaries in the conservative case, and up to  $\max a_{12} \sim 50$  AU for visual binaries in the optimistic case. Thus, the combination of various spectroscopic and interferometric techniques will allow the detection of binaries in the GC with separations ranging from a few stellar radii to several 10 AU.

#### 4.2.2. The red giant binary population in the GC

As argued above, the constraints set by current and forthcoming observational capabilities reduce to three primary requirements: low-mass red giants with  $M_{12} < 4 M_{\odot}$ , a maximal magnitude  $K \lesssim 14$  for SINFONI or  $K \lesssim 16$  for GRAVITY, and a maximal sma  $a_{12} \lesssim 3$  AU for SINFONI or  $a_{12} \lesssim \text{few} \times 10$  AU for GRAVITY. We now estimate the number of detectable low-mass red giant binaries in the GC (the “discovery space”) from the observed  $K$  luminosity function in the GC, for the *null hypothesis*, namely the assumption that the effects of dynamical evolution on the binaries' properties are negligible, and therefore binaries in the GC have the low-mass binary fractions observed in dense Galactic clusters and the low-mass binary period distribution observed in the field.

The  $K$  luminosity function of the red giants in the inner  $\sim 1/2$  pc is well approximated by (Alexander & Sternberg 1999; Bartko et al. 2010)

$$N(< K, R < 1/2 \text{ pc}) \simeq 10^{-2.4+0.35K}, \quad (29)$$

which allows the observed total surface number density of red giants in the GC (Buchholz et al. 2009; Bartko et al. 2010) to be scaled to a given magnitude limit. Assuming the observed and deduced range of binary fractions in galactic clusters and that of massive binaries in the GC,  $F_2 \sim 0.05 - 0.5$ , we estimate that there may be  $N_2 \sim 15-150$  low-mass binaries among the  $N_K \sim 300$   $K < 14$  red giants that are observed within  $1/2$  pc of the MBH, and  $N_2 \sim 80-800$  binaries among the  $N_K \sim 1600$   $K < 16$  red giants there.

A complete survey of low-mass  $M_{12} \simeq 2 M_{\odot}$  field binaries indicates a log-normal orbital period distribution

TABLE 2  
PROPERTIES OF TYPICAL RED GIANTS IN THE GC

Type	$M_{\star}^{1,3}$	$R_{\star}^1$	$T_{\text{eff}}$	$K^2$	$T_{MS}^4$
K2(III)	$2.0 M_{\odot}$	$19 R_{\odot}$	4351 K	15.1	2 Gyr
K5(III)	$1.6 M_{\odot}$	$33 R_{\odot}$	4023K	13.5	4 Gyr
M0(III)	$1.2 M_{\odot}$	$40 R_{\odot}$	3914 K	13.1	7 Gyr
M2(III)	$0.8 M_{\odot}$	$61 R_{\odot}$	3695 K	12.4	12 Gyr

<sup>1</sup> van Belle et al. (1999)

<sup>2</sup> Cox (2000)

<sup>3</sup> Uncertain mass in the range  $0.8 - 2 M_{\odot}$ .

<sup>4</sup> Uncertain main-sequence lifespan in the range  $2 - 12$  Gyr.

with  $\langle \log_{10} P_{12} \rangle = 4.8$  and  $\sigma_{\log_{10} P_{12}} = 2.3$  for  $P_{12}$  in days (corresponding to a median period of  $\simeq 180$  yr) Duquennoy & Mayor (1991). Assuming that the shorter period tail of this distribution applies also in the GC<sup>12</sup>, then the fraction of binaries with  $a_{12} < 2.5$  AU ( $P_{12} < 2.8$  yr) is at least  $F_P = 0.22$ , that of binaries with  $a_{12} < 8$  AU ( $P_{12} < 16$  yr) is at least  $F_P = 0.33$ , and that of binaries with  $a_{12} < 25$  AU ( $P_{12} < 88$  yr) is at least  $F_P = 0.45$ . The number of potential targets in each of these classes is  $N_{2RG} = F_P F_2 N_K$ . We therefore estimate that in the absence of strong dynamical evolution, there may exist in the central  $1/2$  pc of the GC  $N_{2RG} \sim 3 - 30$  low-mass  $K < 14$ ,  $P_{12} < 3$  yr binaries,  $N_{2RG} \sim 25 - 250$  low-mass  $K < 16$ ,  $P_{12} < 8$  yr binaries, and  $N_{2RG} \sim 50 - 500$  low-mass  $K < 16$ ,  $P_{12} < 88$  yr binaries.

Figure (4) shows the observed and derived properties of galactic G, K and M red giants (Gratton et al. 1982; Dumm & Schild 1998), translated to the GC distance and extinction, as function of  $T_{MS}$ , where the main-sequence lifespan was matched by mass to the  $0.8 - 120 M_{\odot}$  Solar metallicity stellar tracks of Schaller et al. (1992) and extrapolated below  $0.8 M_{\odot}$  assuming the low-mass limit relation  $T_{MS} \propto M_{\star}^{-2.5}$  Hansen et al. (e.g. 2004). The  $K$ -magnitude was estimated from the effective temperature. The plot shows that the effective temperature, and hence spectral type, are nearly independent of the mass, and hence  $T_{MS}$ , while the increase of the  $K$ -magnitude with the decrease of mass is substantially smeared by large scatter. It is therefore not possible to determine the stellar mass to better than a factor of  $\sim 2$ , and  $T_{MS}$  to better than a factor of  $\sim 2^{2.5} \sim 6$ . Table (2) lists four low-mass red giants types that are observed in the GC and serve below in examples of the dynamical constraints that can be derived from low-mass red giant binaries. For demonstration purposes, the mass range  $0.8 - 2.0 M_{\odot}$  has been assigned in equal increasing increments from the latest to the earliest types in the table, and likewise the corresponding main-sequence lifespans in equal decreasing logarithmic increments the range  $2 - 12$  Gyr. However it should be emphasized that for all these spectral types the uncertainty in mass and stellar lifespan is such that  $0.8 \lesssim M_{\star} \lesssim 2 M_{\odot}$  and  $2 \lesssim T_{MS} \lesssim 12$  Gyr.

#### 4.2.3. Dynamical constraints by GC red giant binaries

Figure (5 A) shows the binary period, the typical reflex velocity (the actual velocity will depend on projection and the eccentricity), and the softness parameter (assuming  $\alpha = 7/4$

<sup>12</sup> A truncation of the long period tail of the distribution by evaporation will increase the normalization constant relative to the untruncated one. The normalized Duquennoy & Mayor (1991) distribution therefore provides an under-estimate of the actual fraction of shorter-period binaries.

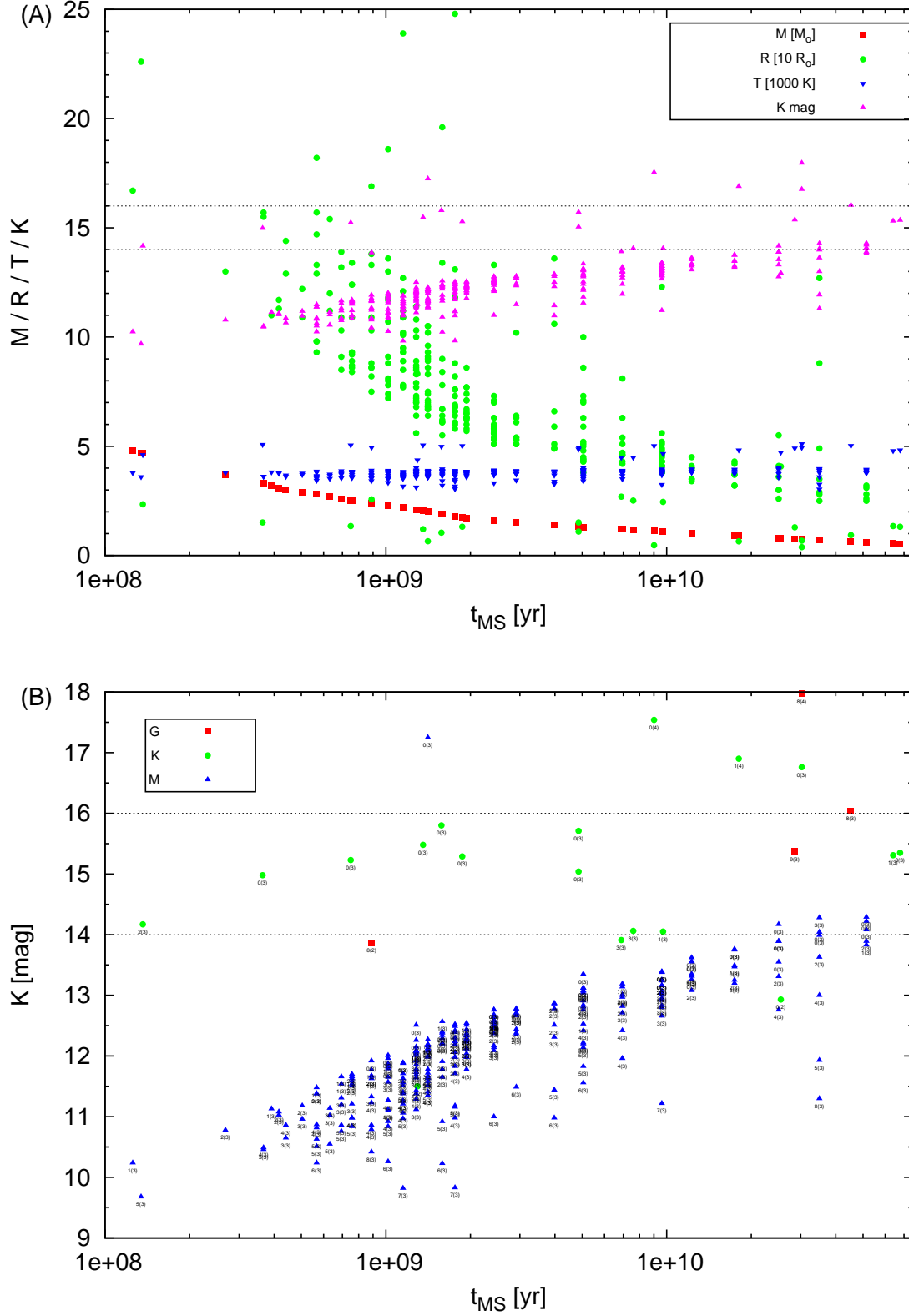


FIG. 4.— The observed and deduced properties of samples of G,K (Gratton et al. 1982) and M (Dumm & Schild 1998) low-mass red giants, translated to the GC ( $DM = 14.6$ ,  $A_K = 2.7$  mag). The main sequence lifetimes were adapted from the Schaller et al. (1992) Solar metallicity stellar tracks between  $M_{\star} = 0.8 M_{\odot}$  to  $120 M_{\odot}$  and extrapolated to lower masses by  $T_{MS}(M_{\star}) = T_{MS}(0.8 M_{\odot})(M_{\star}/0.8 M_{\odot})^{-2.5}$ . (A) The red giant mass, radius, effective temperature and  $K$  magnitude in the GC. (B) The  $K$  magnitudes at the GC for the different spectral types (with the designation of the sub-class and luminosity class in the format “sc(lc)”). The  $K_{S/N} = 14, 16$  thresholds are over-plotted for convenience.

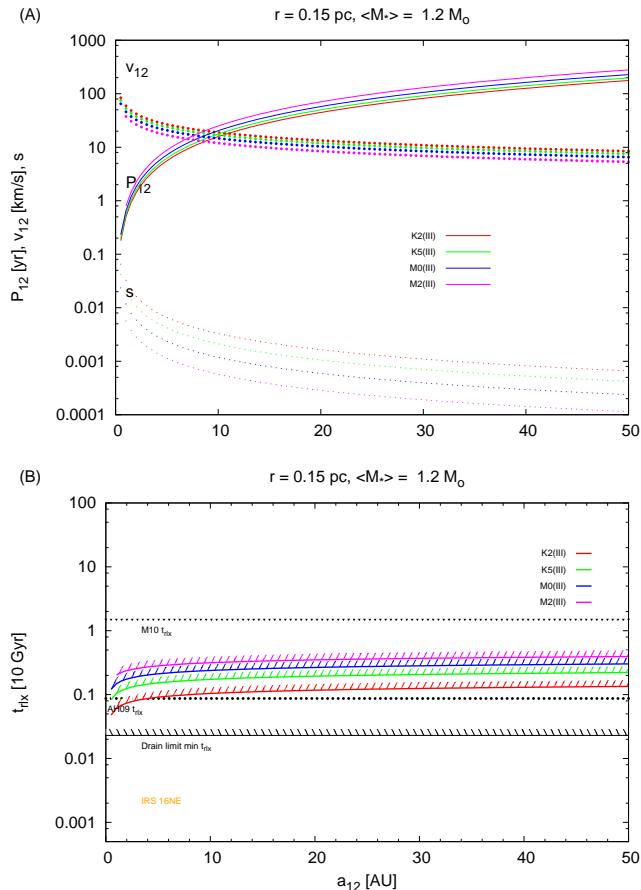


FIG. 5.— (A): The orbital period  $P_{12}$  reflex velocity,  $v_{12}$  and softness parameter  $s$  (for  $\alpha = 7/4$  and  $\langle M_* \rangle = 1.2 M_\odot$ ) at  $r = 0.15$  pc for 4 types of equal mass binaries (Table 2), as function of the binary sma in the range  $a_{12} > 2R_*$ . Over most of the range of interest  $P_{12}$  is short enough and  $v_{12}$  typically high enough for detection. (B): The lower bound on the relaxation timescale,  $\min t_{r1x}$ , which could be inferred from the discovery of a binary at  $r = 0.15$  (Eq. 11).  $\langle M_* \rangle = 1.2 M_\odot$  is assumed based on the GC model of Alexander & Hopman (2009). The allowed values of  $t_{r1x}$  extend above the hashed lines. Three theoretical predictions for  $t_{r1x}(0.15 \text{ pc})$  are shown: The Drain Limit (Alexander & Livio 2004), which provides a lower bound on viable steady-state models, the mass-segregated GC model of Alexander & Hopman (2009), which is similar to that of Freitag et al. (2006), and the post-merger “scoured” GC model of Merritt (2010). Also shown is the bound provided by the recently discovered IRS 16NE. A model that predicts a relaxation time that lies substantially below the lower limit provided by the binaries is ruled out (see discussion in Sec. 5).

and  $\langle M_* \rangle = 1.2 M_\odot$ , cf Figure 2), as function of binary sma above the contact limit  $a_{12} > 2R_*$ , up to  $a_{12} = 50$  AU.

Figure (5 B) compares the lower limits on the relaxation time that can be derived by the detection of such binaries as function of the sma, estimated for  $r = 0.15$  pc, to the various theoretical models. The results show that the detection of such binaries there can rule out that the system is at the drain limit, and can significantly constrain mass-segregated models of the GC. Similarly, Figure (6) shows the lower limits of these binaries at  $a_{12} = 2$  and 50 AU, as function of the distance from the MBH. The results show that because the relaxation times in relaxed models typically decrease toward the center, finding binaries there will provide stronger constraints on the models.

## 5. DISCUSSION AND SUMMARY

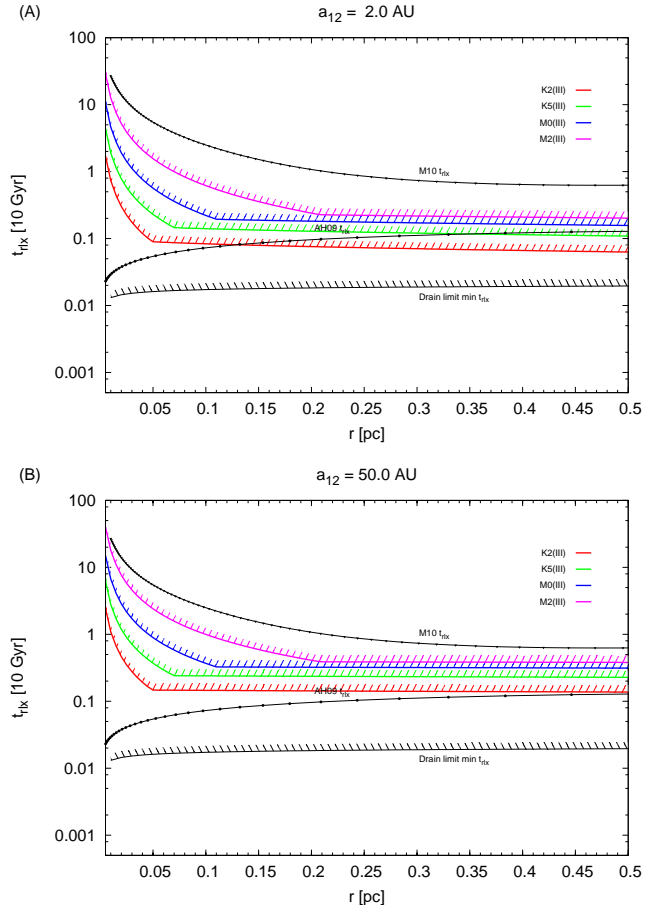


FIG. 6.— Same as in Figure (5 B), but for a fixed binary sma, as function of distance  $r$  from the MBH, and assuming  $\langle M_* \rangle = 0.88(r/1 \text{ pc})^{-0.12}$ , based on the GC model of Alexander & Hopman (2009) (Figure 2). (A) A spectroscopic / astrometric binary with  $a_{12} = 2$  AU. (B) A visual binary with  $a_{12} = 50$  AU.

The detection of long-period binaries in the GC can provide lower limits on the local 2-body relaxation timescale, and correspondingly, upper limits on the number density of the dark cusp that is predicted to exist there. However, since there is no compelling theoretical prediction for the formation or capture rate of binaries there, the converse is not true: the absence of binaries *can not* prove the existence of a high density cusp—it is merely consistent with it.

We have shown that low-mass long-period binaries are already detectable among the brighter red giants in the GC. We adopt the observed statistics of such binaries in dense clusters and their period distribution in the field as the *null hypothesis* (binary formation in the GC is not special, and there is no evaporation), and use these to estimate the number of observable low-mass, long period binaries. Assuming the null hypothesis, and taking into detailed account the VLT’s existing and forthcoming instrumentation and the observational and data analysis constraints, we estimate that among the brighter ( $K < 14$ ) red giants in the central 1/2 pc of the GC there could be  $N_{2RG} \sim 3 - 30$  spectroscopic binaries currently detectable by the integral field spectrometer SINFONI/VLT and  $N_{2RG} \sim 50 - 500$  fainter ( $K < 16$ ) astrometric and visual binaries that could be detected by the forthcoming AO-assisted IR interferometer GRAVITY/VLT. The discovery potential will increase as observations become deeper, the observing

cadence higher, and the monitoring baseline longer. This requires a specifically planned long-term campaign. However, even the presently available data may already include a few long-period binaries.

It is quite likely that the null hypothesis is unrealistic. There are reasons to believe that star formation and binary formation in the unique environment near a MBH proceed quite differently than in less extreme environments. The initial fraction of binaries in the GC could be either much higher or much lower. For example, the dynamics of binary formation in a fragmenting accretion disk possibly leads to a very rapid hardening and merging of binaries (Baruteau et al. 2011). Conversely, the expected high density of compact remnants near the MBH, presumably responsible to the over-abundance of low-mass X-ray binaries there (Muno et al. 2005) suggests the intriguing possibility of exotic binaries composed of a red giant and a stellar mass black hole, which were not considered here.

Since evaporation is a statistical process, robust limits on the dynamical state of the GC require a sample of low-mass long-period binaries. Our estimates of the number of detectable binaries indicate that a dedicated search can plausibly yield at least a small sample, if some binaries do indeed survive in the GC.

Binaries can also be destroyed by processes other than evaporation. This will not affect our method for constraining the dark cusp, which draws conclusions only from those binaries that do survive. This can be stated formally as follows: assume that there are several competing binary destruction processes, which singly would limit a binary's lifetime to  $t_i(\{p_i\})$ , where  $i = 0, 1, 2, \dots$  labels the process (evaporation is process 0), and  $\{p_i\}$  is the set of physical parameters that process  $i$  depends on (e.g.  $n_*$ ,  $\langle M_* \rangle$ ,  $\langle M_*^2 \rangle, \dots$ ), which can be constrained by the detection of surviving binaries. The existence of a binary with age  $T_{12}$  then sets the limit  $T_{12} < \min_i t_i \leq t_0 = t_{\text{evap}}$  irrespective of the relative efficiencies of the processes. However, the presence of multiple binary destruction channels is relevant in that it decreases the chances of finding any usable binaries. We now list some of the competing destruction channels, without committing to specific rates or rank order. We have argued (Pfuhl et al. 2013) that the tidal break-up of a binary by the MBH occurs on a timescale of a few  $\times t_{\text{rlx}} \gg \tau_{\text{evap}}$  (Eq. 10). Tidal breakup driven by incoherent 2-body relaxation will therefore not compete with evaporation, except possibly very near the MBH (Hopman 2009). On the other hand, breakup driven by resonant relaxation could be more efficient, especially very near the MBH (Rauch & Tremaine 1996; Hopman & Alexander 2006), where it could destroy binaries at a rate faster than 2-body relaxation replenishes them (e.g. Madigan et al. 2011). In addition, accelerated binary mergers can be induced by Kozai perturbations by the MBH. This effect is expected to be relevant for the subset of high-inclination orbits close to the MBH (Antonini et al. 2010; Antonini & Perets 2012).

We have shown how the properties of a detected binary: location, mass, period, main-sequence lifespan, and the observed and deduced properties of the GC, the MBH mass and the stellar velocity dispersion, are translated to a lower bound on the 2-body relaxation time  $t_{\text{rlx}}$  (11) and an upper bound on the second moment of the mass distribution,  $n_* \langle M_*^2 \rangle$  (12), *independently of the uncertainties in the binary fraction in the GC*. In concise form, these bounds can be expressed in terms of the observed or derived binary prop-

erties: The main-sequence lifetime  $T_{12}$ , the orbital velocity scale  $v_{12}^2 = GM_{12}/a_{12}$ , the Coulomb logarithm  $\log \Lambda_{12}$  (Eq. 4), and the maximal evolution ratio  $S_h$  (Eq. 6), through the combination

$$X_{12}(r) = \frac{T_{12} \log \Lambda_{12}}{v_{12}^2 S_h(r)}. \quad (30)$$

Together with assumed model values for  $\alpha$ , the logarithmic slope of the stellar cusp,  $\langle M_* \rangle$ , the mean stellar mass, and the observed or modeled velocity dispersion  $\sigma_*$  (Eq. 1), the bounds on the relaxation time and stellar density are

$$t_{\text{rlx}}(r) > 1.4 \frac{\sigma_*^2(r)}{\log(M_\bullet / \langle M_* \rangle)} X_{12}(r),$$

$$n_* \langle M_*^2 \rangle < 0.24 \frac{\sigma_*^2(r)}{G^2} X_{12}^{-1}(r). \quad (31)$$

We have shown that the detection of such binaries could rule out the possibility of a maximally dense relaxed stellar cusp at the drain limit, and constrain more realistic relaxed dynamical models of the GC.

The key issue, and the main source of uncertainty, is to determine how long the binary spent in or near its observed location. The actual age (as opposed to the lifespan) of red giants can be estimated from the main-sequence lifespan of their progenitors,  $T_{MS}$ , which in principle could provide  $T_{12} \sim T_{MS}$  to within 10% (the typical relative duration of the post-main sequence phase). This is different from the case of young massive stars, whose age can only be bound by their main-sequence lifespan,  $T_{12} < T_{MS}(M_*)$ , unless they can be associated with the stellar disk, whose age is known,  $T_{12} \simeq (6 \pm 2) \text{ Myr}$ .

We have argued that local tidal or 3-body formation in the GC is negligible (Sec. 2.3), and therefore the binaries orbiting the Galactic MBH are either primordial and local, or primordial and captured by a 4-body tidal interaction between a hierarchical triple and the MBH (Perets 2009b), in a variation of the Hills (1988) mechanism. The fraction of such captured binaries among the local binaries is uncertain. They will spend a substantial fraction of the post-capture time on very eccentric orbits, until these are randomized (Perets et al. 2009), which may provide a way to identify them if they are relatively recently captured. In any case, under the plausible assumption that both their time of formation and their time of capture are random and distributed uniformly in time over their main-sequence lifespan  $T_{MS}$ , then their mean time in the GC is  $\langle T_{12} \rangle \sim T_{MS}/4$ , which is within the expected uncertainty in the determination of the main-sequence lifetimes of the low-mass red giant binaries (table 2).

The analysis presented here makes several simplifying assumptions, which should be relaxed and calculated in more detail. (1) The estimates here are based on the present-day location of the binary in the GC, without orbital averaging. For long-lived binaries, the evolution of the binary's orbit around the MBH is not negligible and should be also taken into account, as should the evolution of the nuclear cluster itself. (2) The statistical fluctuations in the stochastic process of evaporation are not taken into account. Evaporation should be expressed by survival probabilities, rather than by a single timescale. (3) The estimates are based on the present-day binary parameters  $a_{12}$  and  $M_{12}$  and take into account only the dynamical evolution of soft binaries due to external interactions with stars. However, these parameters also evolve internally because of post-main sequence mass-loss, which is

neglected here. Issues (1) and (2) in particular should be addressed by  $N$ -body modeling of the evaporation process.

Finally, it should be stressed that binary evaporation is insensitive to relaxation by spatially extended massive perturbers (e.g. giant molecular clouds, or dense clusters), which can shorten the relaxation time by many orders of magnitude (Perets et al. 2007), since these will not widen the binary, but rather scatter its center of mass. Thus,  $\max n_* \langle M_*^2 \rangle$  is a limit on the point-like masses in the system (stars, compact remnants and possibly also intermediate-mass BHs), and  $\min t_{\text{rlx}}$  is a lower limit on the *stellar* 2-body relaxation timescale alone. The actual relaxation time due to both stars and extended massive perturbers may be shorter still.

T.A. acknowledges support by ERC Starting Grant No. 202996, DIP-BMBF Grant No. 71-0460-0101, and the I-CORE Program of the PBC and ISF (Center No. 1829/12). T.A. is grateful for the hospitality of the Kavli Institute for Theoretical Physics, UC Santa Barbara, where this work was completed. This research was supported in part by the National Science Foundation under Grant No. NSF PHY11-2591.

## REFERENCES

- Alexander, T. 1999, *ApJ*, 527, 835 1, 2.1  
 —. 2005, *Physics Reports*, 419, 65 1  
 Alexander, T. 2011a, in *ASP Conf. Ser.*, Vol. 439, *The Galactic Center: a Window to the Nuclear Environment of Disk Galaxies*, ed. M. R. Morris, Q. D. Wang, & F. Yuan, 129 1  
 Alexander, T. 2011b, in *Black Holes (STScI 2007 Spring Symp.)*, ed. M. Livio & A. Koekemoer (Cambridge University Press) 1  
 Alexander, T. 2012, in *European Physical Journal Web of Conferences*, Vol. 39, *Tidal Disruption and AGN outburst*, 5001 1  
 Alexander, T., & Hopman, C. 2009, *ApJ*, 697, 1861 1, 2.1, 1, 3, 3.1, 3.2, 1, 4.1, 5, 6  
 Alexander, T., & Kumar, P. 2001, *ApJ*, 549, 948 2.1, 2.3  
 Alexander, T., & Livio, M. 2004, *ApJ*, 606, L21 3.1, 5  
 Alexander, T., & Loeb, A. 2001, *ApJ*, 551, 223 1  
 Alexander, T., & Morris, M. 2003, *ApJ*, 590, L25 1  
 Alexander, T., & Sternberg, A. 1999, *ApJ*, 520, 137 1, 3.2, 4.2.2  
 Amaro-Seoane, P., Gair, J. R., Freitag, M., Miller, M. C., Mandel, I., Cutler, C. J., & Babak, S. 2007, *Classical and Quantum Gravity*, 24, 113 1  
 Antonini, F., Faber, J., Gualandris, A., & Merritt, D. 2010, *ApJ*, 713, 90 5  
 Antonini, F., Lombardi, Jr., J. C., & Merritt, D. 2011, *ApJ*, 731, 128 4.1  
 Antonini, F., & Perets, H. B. 2012, *ApJ*, 757, 27 5  
 Bahcall, J. N., & Wolf, R. A. 1976, *ApJ*, 209, 214 2.1  
 —. 1977, *ApJ*, 216, 883 1, 2.1, 3.2  
 Bailey, V. C., & Davies, M. B. 1999, *MNRAS*, 308, 257 1  
 Bar-Or, B., Kupi, G., & Alexander, T. 2013, *ApJ*, 764, 52 1, 2.2  
 Bartko, H., et al. 2008, in *Society of Photo-Optical Instrumentation Engineers (SPIE) Conference Series*, Vol. 7013, *Society of Photo-Optical Instrumentation Engineers (SPIE) Conference Series* 4.2.1  
 Bartko, H., et al. 2009, *ApJ*, 697, 1741 4.1  
 —. 2010, *ApJ*, 708, 834 1, 3.2, 10, 4.2.2, 4.2.2  
 Baruteau, C., Cuadra, J., & Lin, D. N. C. 2011, *ApJ*, 726, 28 5  
 Benacquista, M. J. 2006, *Living Reviews in Relativity*, 9, 2.3  
 Binney, J., & Tremaine, S. 1987, *Galactic Dynamics* (Princeton, NJ: Princeton University Press) 2  
 —. 2008, *Galactic Dynamics: Second Edition* (Princeton University Press) 2, 2.3  
 Blum, R. D., Ramírez, S. V., Sellgren, K., & Olsen, K. 2003, *ApJ*, 597, 323 1  
 Bonnet, H., et al. 2004, *The Messenger*, 117, 17 4.2.1  
 Buchholz, R. M., Schödel, R., & Eckart, A. 2009, *A&A*, 499, 483 1, 4.2.2  
 Chanamé, J., Gould, A., & Miralda-Escudé, J. 2001, *ApJ*, 563, 793 1  
 Cox, A. N. 2000, *Allen's astrophysical quantities* (New York: AIP Press; Springer, 4th ed.) 2  
 Cvetković, Z., & Novaković, B. 2010, *Astronomische Nachrichten*, 331, 304 4.2.1.0  
 Do, T., Ghez, A. M., Morris, M. R., Lu, J. R., Matthews, K., Yelda, S., & Larkin, J. 2009, *ApJ*, 703, 1323 1  
 Dumm, T., & Schild, H. 1998, *New Astronomy*, 3, 137 4.2.2, 4  
 Duquennoy, A., & Mayor, M. 1991, *A&A*, 248, 485 4.2.2, 12  
 Eisenhauer, F., et al. 2008, in *The Power of Optical/IR Interferometry: Recent Scientific Results and 2nd Generation*, ed. A. Richichi, F. Delplancke, F. Paresce, & A. Chelli, 431–+ 1  
 Eisenhauer, F., et al. 2003, in *Society of Photo-Optical Instrumentation Engineers (SPIE) Conference Series*, Vol. 4841, *Society of Photo-Optical Instrumentation Engineers (SPIE) Conference Series*, ed. M. Iye & A. F. M. Moorwood, 1548–1561 4.2.1  
 Eisenhauer, F., et al. 2011, *The Messenger*, 143, 16 4.2.1  
 Figer, D. F., Rich, R. M., Kim, S. S., Morris, M., & Serabyn, E. 2004, *ApJ*, 601, 319 1, 3.2  
 Freitag, M., Amaro-Seoane, P., & Kalogera, V. 2006, *ApJ*, 649, 91 3.1, 5  
 Fritz, T. K., et al. 2011, *ApJ*, 737, 73 9  
 Gillessen, S., Eisenhauer, F., Trippe, S., Alexander, T., Genzel, R., Martins, F., & Ott, T. 2009a, *ApJ*, 692, 1075 1  
 Gillessen, S., et al. 2009b, *ApJ*, 692, 1075 4.1, 9  
 Goodman, J., & Hut, P. 1993, *ApJ*, 403, 271 2.3  
 Gratton, L., Gaudenzi, S., Rossi, C., & Gratton, R. G. 1982, *MNRAS*, 201, 807 4.2.2, 4  
 Hansen, C. J., Kawaler, S. D., & Trimble, V. 2004, *Stellar interiors: physical principles, structure, and evolution* (Springer-Verlag) 4.2.2  
 Hartkopf, W. I., & Mason, B. D. 2001, *The Sixth Catalog of Orbits of Visual Binary Stars* (US Naval Obs.), <http://ad.usno.navy.mil/wds/orb6.html> 4.2.1.0  
 Heggie, D. C. 1975, *MNRAS*, 173, 729 2.1, 2.1  
 Hills, J. G. 1988, *Nature*, 331, 687 5  
 Hopman, C. 2009, *ApJ*, 700, 1933 1, 2.3, 5  
 Hopman, C., & Alexander, T. 2006, *ApJ*, 645, 1152 1, 5  
 Keshet, U., Hopman, C., & Alexander, T. 2009, *ApJ*, 698, L64 1, 2.1  
 Krabbe, A., et al. 1995, *ApJ*, 447, L95 1  
 Löckmann, U., Baumgardt, H., & Kroupa, P. 2010, *MNRAS*, 402, 519 1  
 Lu, J. R., Do, T., Ghez, A. M., Morris, M. R., Yelda, S., & Matthews, K. 2013, *ApJ*, 764, 155 4.1  
 Madigan, A.-M., Hopman, C., & Levin, Y. 2011, *ApJ*, 738, 99 1, 5  
 Martins, F., Genzel, R., Hillier, D. J., Eisenhauer, F., Paumard, T., Gillessen, S., Ott, T., & Trippe, S. 2007, *A&A*, 468, 233 4.1  
 Martins, F., et al. 2006, *ApJ*, 649, L103 4.1  
 Merritt, D. 2010, *ApJ*, 718, 739 1, 3.3, 5  
 Merritt, D., Alexander, T., Mikkola, S., & Will, C. M. 2010, *Phys. Rev. D*, 81, 062002 1  
 Miller, G. E., & Scalo, J. M. 1979, *ApJS*, 41, 513 3.2, 1  
 Milosavljević, M., Merritt, D., Rest, A., & van den Bosch, F. C. 2002, *MNRAS*, 331, L51 1  
 Morris, M. 1993, *ApJ*, 408, 496 3.1  
 Muno, M. P., Pfahl, E., Baganoff, F. K., Brandt, W. N., Ghez, A., Lu, J., & Morris, M. R. 2005, *ApJ*, 622, L113 5  
 Paumard, T., et al. 2006, *ApJ*, 643, 1011 1, 4.1  
 Perets, H. B. 2009a, *ApJ*, 690, 795 1  
 —. 2009b, *ApJ*, 698, 1330 5  
 Perets, H. B., Gualandris, A., Kupi, G., Merritt, D., & Alexander, T. 2009, *ApJ*, 702, 884 5  
 Perets, H. B., Hopman, C., & Alexander, T. 2007, *ApJ*, 656, 709 1, 2.1, 5  
 Pessah, M., & Melia, F. 2003, *ApJ*, 585, L29 1  
 Pfuhl, O., Alexander, T., Gillessen, S., Martins, F., Genzel, R., Eisenhauer, F., Fritz, T. K., & Ott, T. 2013, in preparation (document), 4.1, 4.2, 5  
 Pfuhl, O., et al. 2011, *ApJ*, 741, 108 1, 10  
 Preto, M., & Amaro-Seoane, P. 2010, *ApJ*, 708, L42 1  
 Rauch, K. P., & Tremaine, S. 1996, *New Astronomy*, 1, 149 1, 5  
 Schaller, G., Schaerer, D., Meynet, G., & Maeder, A. 1992, *A&AS*, 96, 269 2.2, 9, 4.2.1, 4.2.2, 4  
 Schödel, R., et al. 2007, *A&A*, 469, 125 10  
 Sollima, A., Beccari, G., Ferraro, F. R., Fusi Pecci, F., & Sarajedini, A. 2007, *MNRAS*, 380, 781 4.2  
 Sommariva, V., Piotto, G., Rejkuba, M., Bedin, L. R., Heggie, D. C., Mathieu, R. D., & Villanova, S. 2009, *A&A*, 493, 947 4.2  
 Spitzer, L. 1987, *Dynamical evolution of globular clusters* (Princeton, NJ: Princeton University Press, 1987, 191 p.) 2.2  
 Sternberg, A. 1998, *ApJ*, 506, 721 3.2  
 Tohline, J. E. 2002, *ARA&A*, 40, 349 2.3  
 Trippe, S., et al. 2008, *A&A*, 492, 419 2.1  
 van Belle, G. T., et al. 1999, *AJ*, 117, 521 2  
 Weinberg, N. N., Milosavljević, M., & Ghez, A. M. 2005, *ApJ*, 622, 878 1  
 Zucker, S., Alexander, T., Gillessen, S., Eisenhauer, F., & Genzel, R. 2006, *ApJ*, 639, L21 1